

Section 6

**Developments in global forecast models,
case studies, predictability, investigations,
global ensemble, monthly and seasonal
forecasting**

A seasonal re-forecast of mid-latitude circulation over the 20th century

Michel Déqué and Lauriane Batté

Centre National de Recherches Météorologiques (CNRS/GAME), Météo-France.
42 avenue Coriolis F-31057 Toulouse Cédex 1, France, michel.deque@meteo.fr

Preliminary studies in the framework of the European FP7-SPECS research project have shown that the mid-latitude circulation scores of an ensemble forecast are extremely sensitive to the sample of ensemble members. Even with a 50-member ensemble, some uncertainty remains, which can be evaluated from a larger ensemble by random sub-sampling. However, even with a very large ensemble (several hundred members) the forecast score will be representative of the re-forecast period (typically 1979-2012 in SPECS). If the period is short (less than 15 years), the score may poorly estimate the actual predictive skill, because, in the mid-latitudes, the verification is a single realization of a chaotic process (Shi et al., 2015). If the evaluation period is very long (more than 30 years), the re-forecasts include initial conditions of poorer quality (in the ocean and the stratosphere) than in present operational forecasts.

The recent ERA20C reanalysis 1900-2010 (Hersbach et al., 2015) offers the opportunity to test the homogeneity of the scores along the 20th century, and, in case of such a homogeneity, the confidence interval for a score calculated with a re-forecast period of n years. Preliminary attempts using ocean initial conditions derived from flux-driven ocean integrations have shown almost no skill in the first half of the century. Therefore, we use a pseudo-forecast approach with an atmosphere model forced by monthly observed sea surface temperature. The initial conditions, as well as the verification data are extracted from Stream 1 of ERA20C. If we focus on mid-latitude tropospheric general circulation and restrict to forecast months 2 to 4, this method yields, for the last 20 years, similar scores as a fully-coupled model properly initialized. Indeed, the progress in ocean modelling and observation make the prediction of tropical sea surface temperatures during the very first months a well-solved problem. The mid-latitude sea surface temperatures are more difficult to predict, but play a minor role in the large-scale tropospheric circulation in seasonal runs, at least in the present generation of numerical models (Stockdale et al., 2015).

The experimental design is the following. The atmospheric component of CNRM-CM5 (Voldoire et al., 2013) is initialized from 1 Nov. 1900 to 1. Nov. 2010. Sixty model integrations with monthly SST from ERA20C are produced each year until the end of Feb. (4 months). Individual circulation indices are computed for each year, each member, and DJF averages. Then 30-member sub-samples are drawn at random to evaluate the 2.5%, 50%, and 97.5% percentiles of the correlation coefficient. The correlation is calculated for 21-year windows centered at 1910, 1911, ... 2000. This avoids the inclusion of the century trend which could artificially inflate the scores.

NAO (Fig. 1a). This index is calculated as the area-average sea level pressure (SLP) or 500 hPa height geopotential (Z500) difference between 20°N-55°N/90°W-60°E and 55°N-90°N/90°W-60°E. The correlation is higher with SLP during the first half of the century, then higher with Z500, reaching 0.60 in the last decade. The most salient feature is the multidecadal variability: the scores decrease from 1900 to 1970, then increase. Shorter increase phases can be observed in 1900-1910 and 1950-1960. Changes in the observation network used for the atmospheric reanalyses could explain part of this inhomogeneity, but certainly not the 70-year decrease phase obtained. This feature is not due to sampling, because the 95% interval due to the choice of the members excludes the possibility of a constant correlation. Note that the 2.5% and 97.5% percentiles (shaded area), which were originally as noisy as the 50% percentile (solid line), have been filtered by a 9-point parabolic filter for the sake of clarity. At this stage, we can claim that the low predictability of the NAO in 1960-1980 is not an artifact. However we cannot tell yet if this feature is a natural phenomenon, independent of the model.

NAM (Fig 1b): This index corresponds to 34°N-36°N minus 64°N-66°N zonal averages. It is often considered as an extension of the NAO, but the seasonal scores for a given 20-year period may be different. However, the increasing and decreasing phases we got for the NAO are found again here.

SAM (Fig 1c): This index corresponds to 39°S-41°S minus 64°S-66°S zonal averages. It is almost symmetrical to NAM. We are in austral summer, but this is the season of ENSO peaks, and the summer SAM is as predictable as the winter SAM (this feature is different with NAM or NAO which have low scores in boreal summer). The multi-decadal trends are almost opposite to NAM/NAO, with a 0.80 correlation maximum in the 1960s.

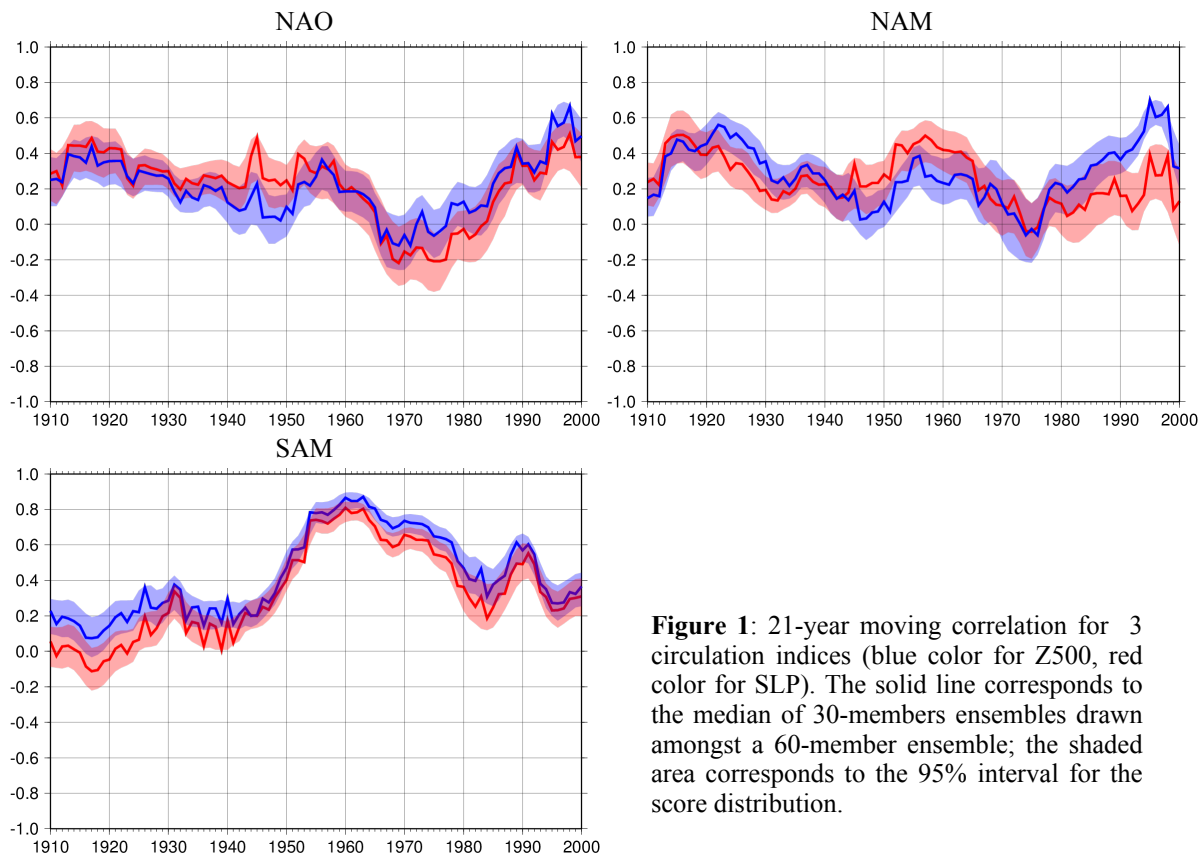


Figure 1: 21-year moving correlation for 3 circulation indices (blue color for Z500, red color for SLP). The solid line corresponds to the median of 30-member ensembles drawn amongst a 60-member ensemble; the shaded area corresponds to the 95% interval for the score distribution.

These results suggest that seasonal predictability of mid-latitude circulation is not constant during the 20th century. This implies that in future decades, seasonal re-forecast scores may decline in the northern hemisphere, notwithstanding scientific progress in the representation of the mid-latitude circulation at this time scale. In the meantime, the variability and uncertainties of such correlation scores show that results in seasonal forecast assessments over these regions should be interpreted with caution.

Acknowledgements : We are thankful to ECMWF for providing the new ERA20C reanalysis over the whole 20th century. Scientific analysis have been carried in the framework of the FP7-SPECS project of the European Commission (grant agreement 308378).

References:

- Hersbach, H., C. Peubey, A. Simmons, P. Berrisford, P. Poli and D. Dee, 2015. ERA-20CM: a twentieth century atmospheric model ensemble. *Quart. J. Roy. Meteorol. Soc.*, in press, DOI: 10.1002/qj.2528
- W. Shi, N. Schaller, D. MacLeod, T. N. Palmer and A. Weisheimer, 2015. Impact of hindcast length on estimates of seasonal climate predictability, in press, DOI: 10.1002/2014GL062829
- Stockdale, T.N., F. Molteni and L. Ferranti, 2015. Atmospheric initial conditions and the predictability of the Arctic oscillation. *Geophysical Res. Letters*, 42, 1173–1179, DOI: 10.1002/2014GL062681
- Voltaire, A. E. Sanchez-Gomez, D. Salas y Mélia, B. Decharme, C. Cassou, S. Sénési, S. Valcke, I. Beau, A. Alias, M. Chevallier, M. Déqué, J. Deshayes, H. Douville, E. Fernandez, G. Madec, E. Maisonnave, M.-P. Moine, S. Planton, D. Saint-Martin, S. Szopa, S. Tyteca, R. Alkama, S. Belamari, A. Braun, L. Coquart and F. Chauvin., 2013, The CNRM-CM5.1 global climate model : description and basic evaluation, *Clim. Dyn.*, DOI:10.1007/s00382-011-1259-y.

Application of Method for Object-Based Diagnostic Evaluation to GFS, GFSX, and ECMWF Precipitation Verification

Tracey Dorian, Fanglin Yang
(Email: tracey.dorian@noaa.gov)
IMSG - NOAA/NCEP/EMC

Introduction:

Forecast verification is a key step to improving model performance. Traditional verification measures offer forecast quality assessment scores, but do not provide diagnostic information about why forecast skill was high or low and traditional verification approaches penalize forecasts twice for missing observed precipitation and for giving a false alarm (Gilleland 2009). Additionally, measures-based verification measures “tend to favor smoother forecast fields of coarser-resolution models” and therefore do not provide useful information on the benefits of high resolution models (Wolff 2014). Object-based precipitation verification, unlike traditional skill scores, offers spatial information about how close the precipitation forecasts are to the observations in location, size, orientation, and intensity. The Method for Object-Based Diagnostic Evaluation (MODE), developed by the National Center for Atmospheric Research (NCAR) Developmental Testbed Center (DTC), is an example of a verification tool that provides statistics about the spatial differences between forecast objects and observation objects. Precipitation objects are defined in both forecasts and observations based on two parameters, the accumulation threshold and a smoothing radius (Davis 2006). Examples of diagnostic information that can be obtained from MODE include centroid distance, angle difference, area ratio, percentile intensity ratio, and more.

Methods:

MODE precipitation verification was applied to three global numerical weather prediction models – the ECMWF, GFS, and GFSX (Parallel GFS) – to the 2014 seasons. Multiple thresholds combined with a fixed smoothing radius were used to compare model forecasts to observations. The 00Z forecasted 24-hour precipitation accumulations ending on the 36, 60, 84, 108, 132, 156, and 180 forecast lead times from the models were compared to Climatologically Calibrated Precipitation Analysis (CCPA) observations. The Median of the Maximum Interest with respect to observation objects (MMIO) is an output summary statistic generated for each MODE run. Larger values of MMIO indicate higher interest values which imply better matches across forecast and observation fields.

Results:

For all four seasons in 2014, the ECMWF generally has the largest MMIO values during most forecast hours. The Parallel GFS has higher MMIO values compared to the T574 GFS. In the summer, the MMIO values are lowest compared to other seasons, and there seems to be a larger drop in MMIO values with forecast lead time. Also in the summer, the MMIO values drop quicker as threshold increases compared to winter, spring, and fall. All three models consistently overestimate the extreme light rain intensities, or the 10th and 25th percentile intensities, averaged over all forecast hours. The median light rain intensities in the GFSX, however, do appear to be closest to observations during all four seasons. For median intensities, or 50th percentile intensities, all three models do quite well throughout the entire year. The GFSX is farthest from observations in summer where it underestimates the intensities. For the

extreme high intensities, or the 75th and 90th percentile intensities, the three global models generally underestimate intensities and are farthest from observations in late winter/early spring and in the summer. The GFSX intensities, once again, are usually closest to observations in 2014. The variation in model bias from day to day is much larger for the 75th and 90th percentile intensities compared to the lower percentile intensities. Similarly, the variation in median percentile intensities between forecast lead times is larger for heavy rain. The GFSX is closest to observations in total object count, especially in summer where the GFS and ECMWF largely underestimate the number of objects - the same is true for fall 2014. For winter and spring of 2014, the GFSX overestimates total object count. The GFS appears closest to observations in total object count in the spring. Finally, for all seasons in 2014 the European model and GFS median object areas are larger than observations during most forecast lead times. The Parallel GFS is closest to observations for the median object area, but also tends to forecast larger object areas compared to observations during all seasons.

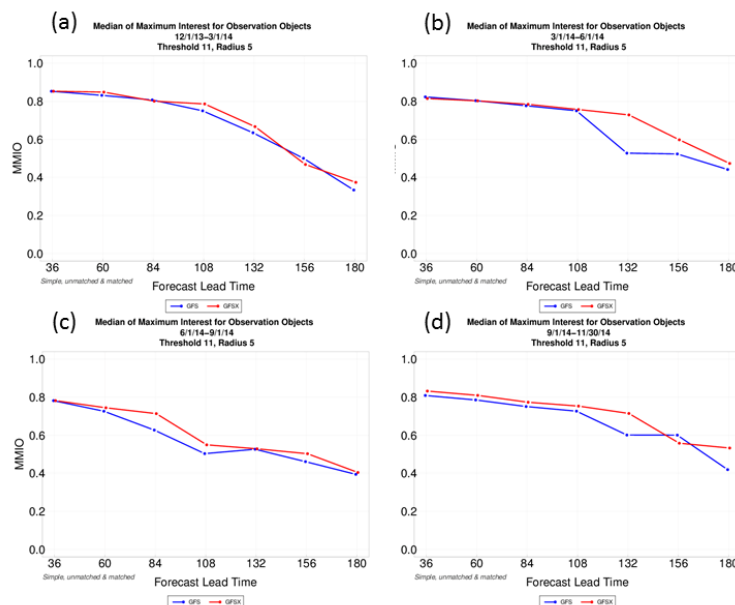


Figure 1: The Median of Maximum Interest for observation objects versus forecast lead time for accumulation threshold 11mm and convolution radius of 5 grid squares for (a) winter 2013-2014, (b) spring 2014, (c) summer 2014, and (d) fall 2014. T575 GFS is in blue, GFSX T1534 is in red. Forecasts are for 24-h accumulated precipitations ending on x-axis forecast lead times.

References:

Davis, C. et al. (2006): Object-Based Verification of Precipitation Forecasts. Part I: Methodology and Application to Mesoscale Rain Areas. *Monthly Weather Review.*, 134, 1772-1784. doi: <http://dx.doi.org/10.1175/MWR3145.1>

Gilleland, E. et al. (2009): Intercomparison of Spatial Forecast Verification Methods. *Weather and Forecasting.*, 24., 1416-1430. doi: <http://dx.doi.org/10.1175/2009WAF2222269.1>

Wolff, J.K. et al. (2014): Beyond the Basics: Evaluating Model-Based Precipitation Forecasts Using Traditional, Spatial, and Object-Based Methods., *Weather and Forecasting.*, 29., 1451-1472. doi: <http://dx.doi.org/10.1175/WAF-D-13-00135.1>

Challenges and Opportunities in Modeling of the Global Atmosphere

Zavisa Janjic, Vladimir Djurdjevic, Ratko Vasic, and Tom Black
NOAA/NCEP/EMC, College Park, MD 20740, U.S.A.
(Email: zavisa.janjic@noaa.gov)

Progress in atmospheric modelling has always been related to advances in computer technology. The unprecedented computer power that is now available allows operational application of horizontal resolution on the order of 10 km on the global scale. However, the current parallel computer architecture requires that some widely adopted modeling paradigms be reconsidered in order to productively utilize as much of the power of parallel processing as possible.

For example, with parallel processing using distributed memory, each core may work on a small subdomain of the full integration domain, and only exchange few rows of halo data with the neighbouring cores in order to specify the lateral boundary conditions they need. This scenario promises good scaling because the communications are restricted only to the halo exchanges between neighboring cores. However, note that the described simplified scenario implies that all the discretization algorithms used in the model are Eulerian and horizontally local. Unfortunately, such algorithms do not include those using spectral representation and semi-implicit time differencing which require much more communications and therefore cannot scale as well. Without the semi-implicit scheme the semi-Lagrangian approach may become prohibitively computationally expensive.

Still, a wide freedom of choice is left to modellers designing limited area models. However, on global scales the treatment of spherical geometry remains an issue. The straightforward latitude-longitude grid with local in space and explicit in time differencing was a natural early choice in the sixties, and has remained in use ever since. The problem with this method is that the grid size in the longitudinal direction tends to zero as the poles are approached due to the convergence of the meridians. So in addition to having unnecessarily high resolution near the poles, polar filtering has to be applied in order to keep the integration stable using a decent-sized time step. However, the polar filtering based on conventional fast Fourier transforms requires transpositions involving extra communications and thus limits scaling.

The discovery of the spectral transform method in early seventies, and the development of the semi-implicit semi-Lagrangian schemes in the eighties, opened the way for a wide application of the spectral representation in global models. With some variations, these techniques are still used operationally and for research at most major centers. However, in addition to spectral ringing, two-dimensional non-locality is inherent to the spectral representation and implicit time differencing, which is often considered to be a bottleneck inhibiting scaling on a large number of cores. In this respect the lat-lon grid with fast Fourier transforms represents a significant step in the right direction.

Other grid topologies with reduced variability of the grid distances were also considered at an early stage. Among these were, for example, the cubed sphere and the hexagonal/pentagonal “soccer ball” grids that were pioneered in the sixties. These grids suffered from inhomogeneities that could result in developing large – scale (wavenumbers 4 and 5) fictitious solutions (“grid imprinting”) with significant amplitudes. Due to their large scales that are comparable to the scales of the dominant Rossby waves, such fictitious

solutions are hard to identify and remove. Examples of the fictitious solutions obtained in the Southern Hemisphere using a cubed sphere and “soccer ball” grids with the resolution of about 10 in the Jablonowski and Williamson (2006) idealized baroclinic development test are shown in Figs. 1 – 2 together with the solutions on the lat – lon grid. So these types of grids did not gain much popularity in the past. However, recently the interest in such grids has been revived by the hope that their problems can be alleviated or eliminated with higher resolutions and more refined grid definitions. Unfortunately, the results of the runs using resolutions of ~ 0.250 and ~ 0.1250 shown in Figs. 3 – 4, do not inspire confidence that the increase in resolution alone will be sufficient.

Another challenge on the global scale is that the limit of validity of the hydrostatic approximation is rapidly being approached. Keeping in mind the sensitivity of extended deterministic forecasts to small disturbances, we may need global non-hydrostatic models sooner than we think, and that is likely to bring additional problems with the computational efficiency of nonlocal schemes.

As a recent example of a multi-scale model, consider the unified Nonhydrostatic Multiscale Model on the Arakawa B grid (NMMB) that is being developed for spatial scales ranging from meso to global at the National Centers for Environmental Prediction (NCEP) as a part of the new NOAA Environmental Modeling System (NEMS) (Janjic and Gall 2012). The model follows the general modeling philosophy of the older NCEP WRF NMM grid-point regional dynamical core. The nonhydrostatic dynamics were designed in such a way as to avoid overspecification. The global version has been run mostly on the latitude-longitude grid, but work on an advanced cubed sphere option is under way as well (Rancic et al. elsewhere in this volume). The regional version uses a rotated latitude-longitude grid to reduce the variation of the grid size.

The model formulation has been successfully tested at various scales. The regional version of the NMMB replaced the WRF NMM as the main NCEP operational short range forecasting model for North America (NAM), as well as in a number of high resolution nested runs. The work on upgrading the NCEP operational Hurricane WRF (HWRF) from the WRF NMM to NMMB dynamics is under way. The latitude-longitude global NMMB has been run in parallel in order to test it. The system is initialized and verified using the spectral analyses of NCEP’s Global Forecasting System (GFS). Nevertheless, the skill of the medium range forecasts produced by the NMMB was comparable to that of other major medium range forecasting systems. As an illustration of the performance of the model, one year average global anomaly correlation coefficient at 500 hPa of the NMMB (red line) and GFS (black line) for the 00 Z runs are shown in Fig. 5 as functions of forecast time.

REFERENCES

- Jablonowski, Christiane, and David L Williamson, 2006: A baroclinic instability test case for atmospheric model dynamical cores. *Quarterly Journal of the Royal Meteorological Society*, **Vol. 132**, 621C, 2943-2975.
- Janjic, Z., and R.L. Gall, 2012: Scientific documentation of the NCEP nonhydrostatic multiscale model on the B grid (NMMB). Part 1 Dynamics. NCAR Technical Note NCAR/TN- 489+STR, DOI: 10.5065/D6WH2MZX .

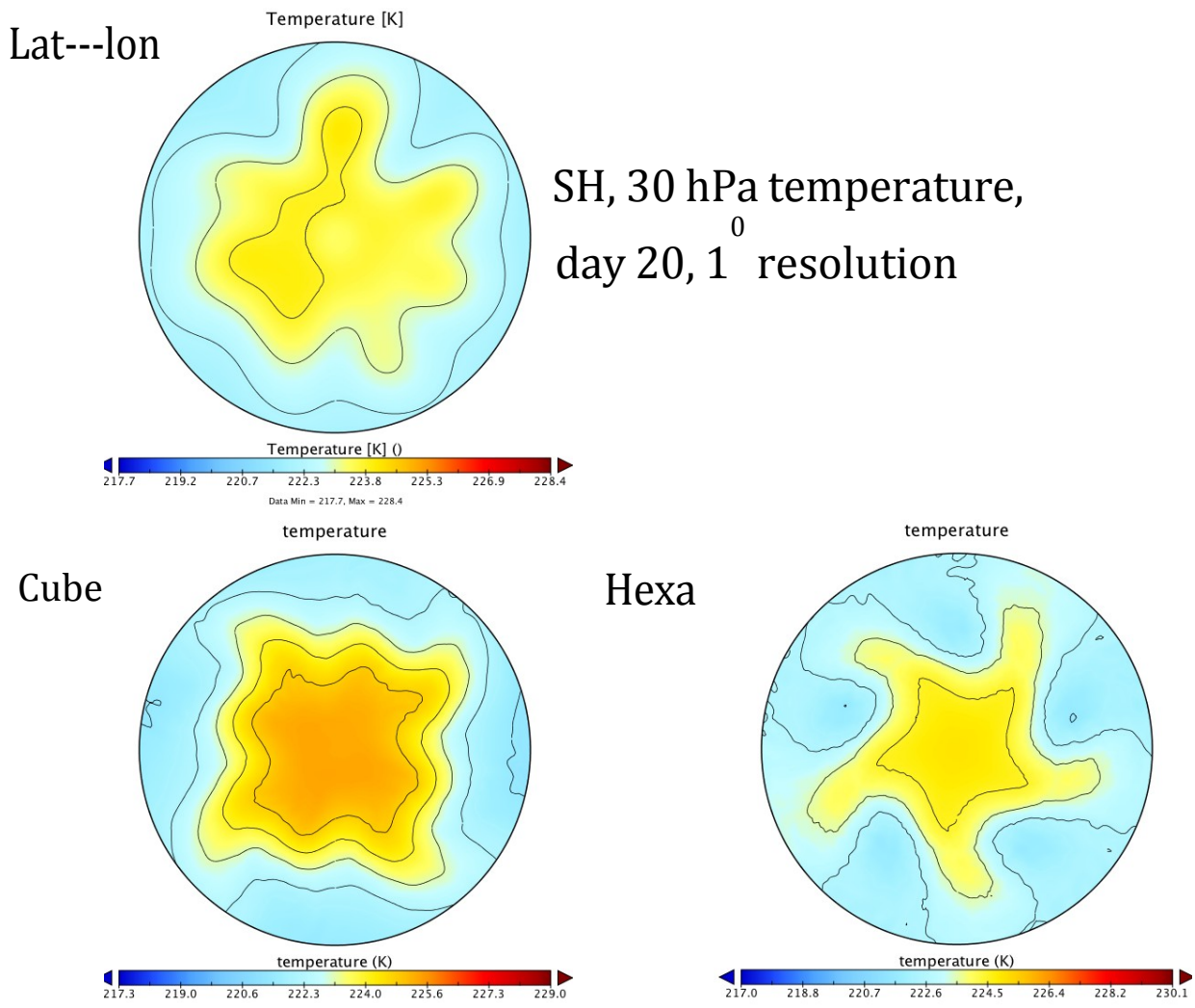


Fig. 1. Temperature at 30 hPa over the Southern Hemisphere after 20 days of integration using the lat-lon grid (upper left), a cube grid (lower left) and a “soccer ball” grid (lower right) with $\sim 1^0$ resolution.

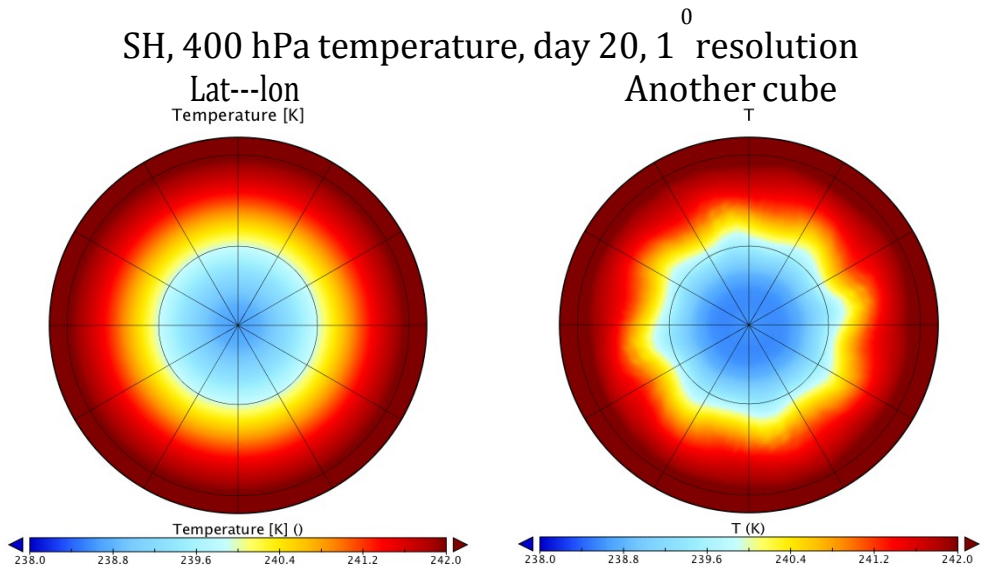


Fig. 2. Temperature at 400 hPa over the Southern Hemisphere after 20 days of integration using lat-lon grid (left), and a cube with Galerkin discretization (right) with $\sim 1^{\circ}$ resolution.

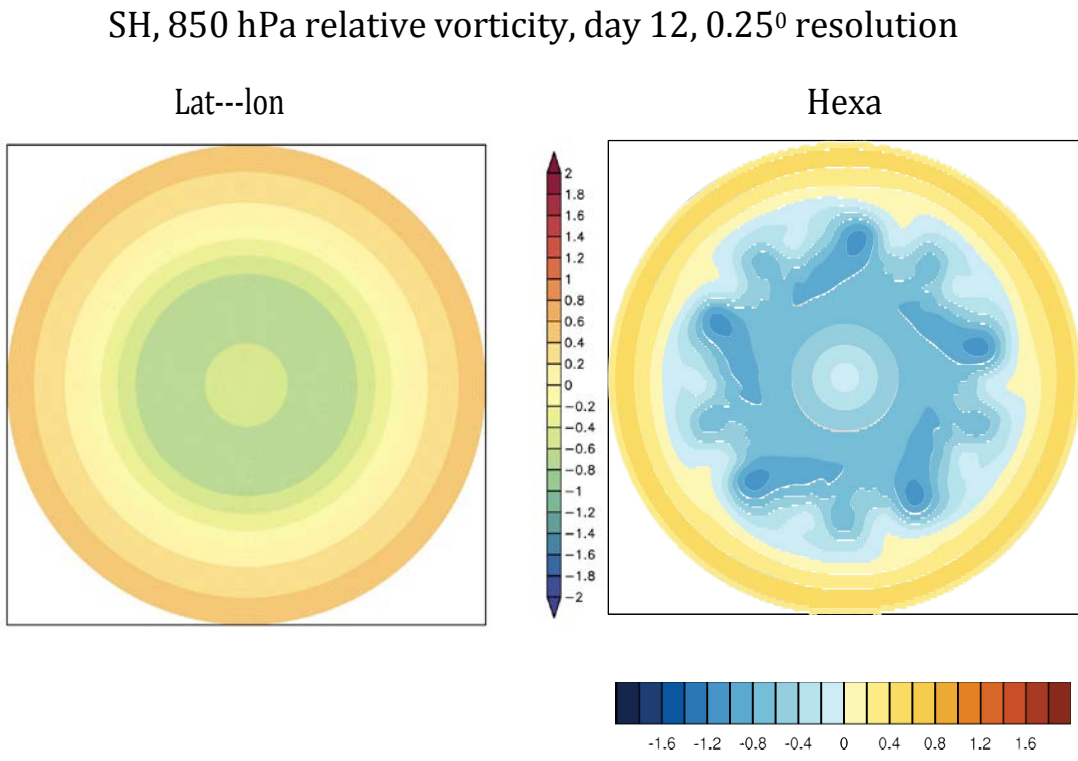


Fig. 3. Relative vorticity at 850 hPa over the Southern Hemisphere after 12 days of integration using the lat-lon grid (left) and a “soccer ball” grid (right) with $\sim 0.25^{\circ}$ resolution.

SH, surface pressure, day 20, 0.125° resolution, cube

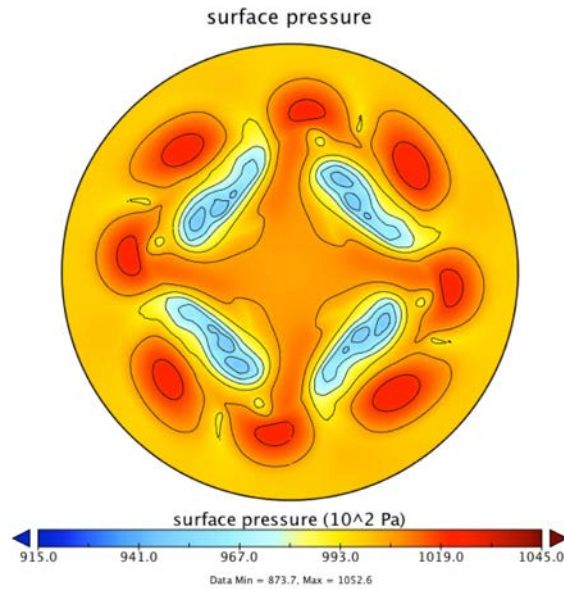


Fig. 4. Surface pressure over the Southern Hemisphere after 20 days of integration using a cube grid with $\sim 0.125^\circ$ resolution.

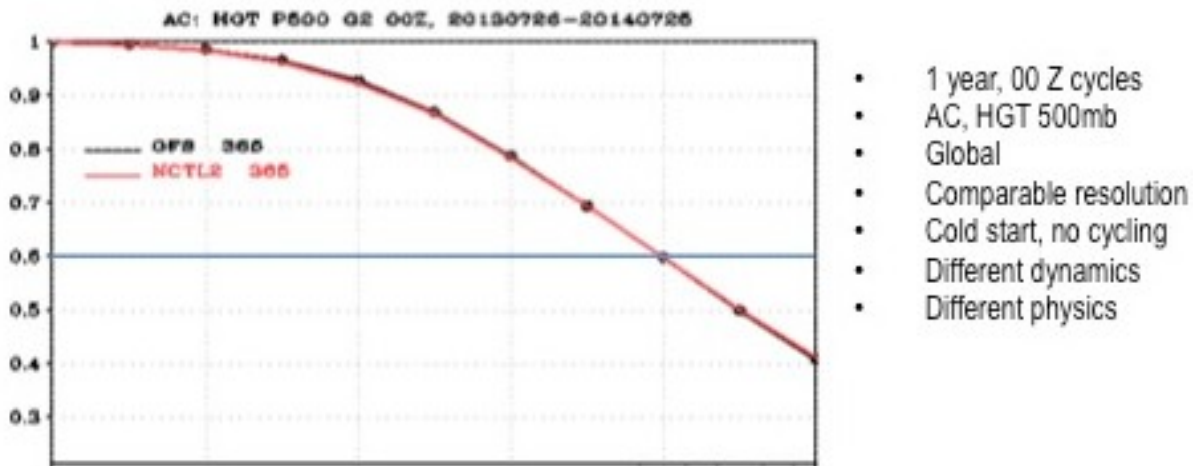


Fig. 5. One year average of global anomaly correlation coefficients at 500 hPa of the NMMB (red line) and GFS (black line) for the 00 Z runs as a function of forecast time.

Uniform-Jacobian Cubic Grid for Efficient Global Modeling

Miodrag Rančić, R. James Purser, Dusan Jović, Ratko Vasić, Zavisla Janjić, Thomas Black,
and Geoff DiMego.

NOAA/NCEP/EMC, College Park, MD 20740, U. S. A.

(Email: miodrag.rancic@noaa.gov)

1. IMPLICATIONS OF THE MASSIVE-PARALLELISM OF MODERN SUPER-COMPUTERS

In order to satisfy the demand for ever faster rates of computation in numerical weather prediction and similarly computationally-intensive tasks, the last two decades have seen the emergence of massively-parallel architectures as the dominant computational paradigm for these activities. Many traditional approaches to weather modeling, proven to be efficient for the older monolithic computer architectures (such as spectral and semi-implicit methods, that required long-range or global communication among the discretized variables of the model every time-step) are now placed at a severe disadvantage in the new massively-parallel context compared to alternative numerical methods designed to avoid all immediate long-range interactions. Not only do these considerations tend more to favor grid-point models over spectral, and explicit dynamics over semi-implicit, but, among grid frameworks, favor those grid configurations possessing a high degree of spatial uniformity that minimize the amount of necessary additional filtering demanded by the requirements of stability and the maintenance of approximate spatial homogeneity.

2. POLYHEDRAL GRIDS

Grids based upon the various ways one can map the surface of a regular griddable polyhedron (e.g., a cube or icosahedron) to the surface of the sphere, have therefore become increasingly popular within the numerical weather modeling community; these grids automatically avoid the strong polar singularity, as well as the need for extensive zonal filtering, associated with the otherwise attractive latitude-longitude computational grid framework. While it is topologically impossible to avoid having localized coordinate singularities at the corners of a continuous polyhedral grid, Rančić et al. (1996), Purser and Rančić (1998) and Tomita et al. (2001) described various techniques by which at least the “edge” singularities of a polyhedral grid are eliminated while elsewhere the smoothness of the grid, except only at the corner singularities, can be guaranteed. Generally, in designing a smooth polyhedral grid, a compromise is made between the degree of local grid distortion, including non-orthogonality, on the one hand, and smooth homogeneity of resolution, on the other, and this compromise can be made explicit in a variational formulation of the problem, as was done in Purser and Rančić (1998). If we opt for the extreme limiting choice of perfect uniformity of (areal) resolution in this context, the result is a polyhedral grid (see figure) with the least distortion possible subject to the overriding constraint of a uniform mapping jacobian; it is this choice of grid that we refer to as the “Uniform-Jacobian cubic” (UJ-cubic) grid when the polyhedron in question is the cube.

3. PUTTING THE NMMB MODEL ON THE UJ-CUBE

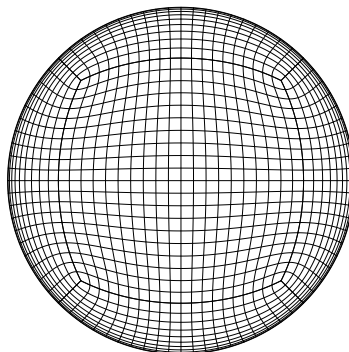


Figure 1. A coarse gridding of the Uniform-Jacobian cube.

We have developed a procedure, described in Purser and Rančić (2011), by which a satisfactory approximation to the UJ-cubic ideal grid can be numerically generated and have adapted a version of the NMMB three-dimensional explicit Eulerian nonhydrostatic forecasting model described in Janjić and Gall (2012) to take advantage of this grid framework. The dynamical core run on the new cubic grid exhibits a significant computational performance advantage compared with the version run on the latitude-longitude grid framework at a similar resolution. This advantage owes to two factors: firstly, the distribution of the horizontal grid points is more uniform over the surface of the sphere; and secondly, there is now no need to run a zonal Fourier filter at high latitudes needed by the latitude-longitude grid model to remove unwanted scales in order to prevent the violation of the CFL stability criterion. While some special numerical procedures are still evidently needed to prevent minor spurious numerical effects from occurring at the eight corners, these potential effects are narrowly confined to the immediate vicinity of each corner and their remedies (localized filtering and modifications to the numerical differencing stencils) are not of a kind that significantly impact the model performance.

REFERENCES

- | | | |
|--|------|---|
| Janjić, Z., and R. Gall | 2012 | Scientific documentation of the NCEP nonhydrostatic multiscale model on the B grid (NMMB). Part I, Dynamics. NCAR Technical Note 489 (NCAR/TN-489 +STR). |
| Purser, R. J., and Rančić, M. | 2011 | A standardized procedure for the derivation of smooth and partially overset grids on the sphere, associated with polyhedra that admit regular griddings of their surfaces. Part I: Mathematical principles of classification and construction. NOAA/NCEP Office Note 467. |
| Purser, R. J., and M. Rančić | 1998 | Smooth quasi-homogeneous gridding of the sphere. <i>Quart. J. Roy. Meteor. Soc.</i> , 124 , 637–647. |
| Rančić, M., R. J. Purser, and F. Mesinger | 1996 | A global shallow-water model using an expanded spherical cube: Gnomonic versus conformal coordinates. <i>Quart. J. Roy. Meteor. Soc.</i> , 122 , 959–982. |
| Tomita, H., Tsugawa, M., Satoh, M., Goto, K. | 2001 | Shallow water model on a modified icosahedral geodesic grid by using spring dynamics. <i>J. Comp. Phys.</i> , 174 , 579–613. |